Journal of Magnetism and Magnetic Materials 498 (2020) 166167

Contents lists available at ScienceDirect

Journal of Magnetism and Magnetic Materials

journal homepage: www.elsevier.com/locate/jmmm

Research articles

Behavior of nanocomposite consisting of manganese ferrite particles and atomic layer deposited bismuth oxide chloride film

Kaupo Kukli[a,b,*], Mats Mikkor[a], Andris Šutka[c], Mikk Kull[a], Helina Seemen[a], Joosep Link[d], Raivo Stern[d], Aile Tamm[a]

[a] Institute of Physics, University of Tartu, W. Ostwaldi 1, 50411 Tartu, Estonia
[b] Department of Chemistry, University of Helsinki, P.O. Box 55, 00014 Helsinki, Finland
[c] Riga Technical University, Faculty of Materials Science and Applied Chemistry, Research Laboratory of Functional Materials Technologies, Paula Valdena 3/7, Riga LV-1048, Latvia
[d] National Institute of Chemical Physics and Biophysics, Akadeemia tee 23, 12618 Tallinn, Estonia

A B S T R A C T

Nanocomposites of manganese ferrite and bismuth oxide chloride were synthesized. The composites consisted of 10 nm thick nanocrystalline bismuth oxide chloride thin film grown by atomic layer deposition on spinel $MnFe_2O_4$ nanoparticles prepared by wet chemical synthesis. The composite layers exhibited nonlinear polarization behavior in both magnetic and electric fields at room temperature. The magnetic coercive force, H_C, was 30–40 Oe at room temperature. The width of electrical charge – voltage hysteresis loop reached 3.6 MV/cm.

1. Introduction

Composite metal oxides of various morphology and structure, including those containing spinel ferrites, MFe_2O_4 (M = Co, Ni, Mn, Mg, etc.) are of interest due to their valuable physical properties allowing electrical insulation, high permeability for magnetic field, and moderate, but rapid magnetization. Such materials in thin film form can be used in, e.g., high frequency transformers, filters, or isolators. In the form of nanoparticles, they can become applied in biomedicine, e.g., in cancer remediation therapies, and, in the form of heterostructures, in a range of composite architectures with functionalities defined by the connectivity between constituent phases [1,2]. It is desirable to produce such nanomaterials at low temperatures via sufficiently robust and cost-effective routes. Manganese ferrite, $MnFe_2O_4$, is one of the iron spinels which is studied in thin film and bulk forms as the material otherwise applied in the microwave and magnetic recording applications characterized by high impedance and low core loss [2]. Earlier, in magnetic core memories, manganese ferrite based materials, such as $Mg_{0.45}Mn^{2+}_{0.55}Mn^{3+}_{0.23}Fe_{1.77}O_4$, have been applied owing to their high coercivity and squareness in magnetization-field loops [3]. $MnFe_2O_4$ particles have also been synthesized and studied for the development of magnetic resonance imaging methods [4], sensors for cancer detection [5] or magnetically guided drug delivery agents [6].

Routes to $MnFe_2O_4$ nanoparticles have largely been based on the wet chemical synthesis, e.g., through reverse micelles techniques using various surfactants [6–9]. High-quality $MnFe_2O_4$ nanocrystals could be synthesized through a seed-mediated non-hydrolytic growth process [10] or a thermal decomposition method [11] using manganese(II) acetylacetonate, $Mn(acac)_2$, and iron(III) acetylacetonate, $Fe(acac)_3$, as metal precursors. Experiments on co-precipitation of $MnFe_2O_4$ particles from iron (III) chloride hexahydrate, $FeCl_3{\cdot}6H_2O$ and manganese(II) chloride $MnCl_2{\cdot}4H_2O$ [12] have also been successfully carried out.

Reports on manganese ferrite based heterostructured composites involving foreign metal oxide layers are rather scarce. There is, for instance, a study devoted to mixed spinel–perovskite composites of $xMnFe_2O_4$ –(1–x)$BiFeO_3$ prepared by a solid state reaction method [13]. In another study templated structure was realized, tailoring useful properties of $BiFeO_3$ and $CoFe_2O_4$ in self-assembled nanocomposites [14]. The latter structures comprised chemically quite pure component oxides laser ablated from two different targets of $Bi_{1.2}FeO_3$ and $CoFe_2O_4$ at rather high temperatures, 580–650 °C, and deposited on (0 0 1) oriented Nb-doped $SrTiO_3$ [14]. In such composites, $BiFeO_3$ promoted ferroelectric behavior, whereas the role for $CoFe_2O_4$ was in the introduction of ferromagnetism in the composite. Bismuth oxide alone has scarcely been applicable as a material potentially capable to polarize saturatively in external fields. One recent study, however, describes ferromagnetic-like behavior observed in nickel-doped bismuth oxide chloride films [15].

The present study is devoted to the examination of a simple route to nanocomposite of manganese iron oxide and bismuth oxide (chloride).

* Corresponding author.
E-mail address: kaupo.kukli@ut.ee (K. Kukli).

https://doi.org/10.1016/j.jmmm.2019.166167
Received 7 May 2019; Received in revised form 19 October 2019; Accepted 16 November 2019
Available online 18 November 2019
0304-8853/ © 2019 The Authors. Published by Elsevier B.V. This is an open access article under the CC BY-NC-ND license (http://creativecommons.org/licenses/by-nc-nd/4.0/).

The goal of the study was the synthesis of $MnFe_2O_4$ nanocrystals with well-defined structure and, thereafter, conformal coating of the crystallites with thin bismuth-based films at a moderate process temperature, in order to examine the primary magnetic and electrical behavior of the composite layer. Manganese iron oxide particles were prepared by wet chemical synthesis, and were thereafter covered by bismuth oxide chloride based thin films by atomic layer deposition.

2. Experimental details

$MnFe_2O_4$ nanoparticles were prepared by wet chemical synthesis and distributed over substrate surface by spin-coating. 2.5 mmol $Mn(NO_3)_3{\cdot}6H_2O$ + 5 mmol $Fe(NO_3)_3{\cdot}9H_2O$ were dissolved in 25 mL of distilled water and added 25 mL 5 M NaOH water solution. Precipitates formed immediately after mixing two solutions. In the next step, precipitates were washed on a filter by filtering 100 mL of distilled water for 3 times. Further, precipitates (without drying) were dispersed in 40 mL of 10 M NaOH water solution. In the next step, suspension was poured in teflon sealed stainless steel autoclave with total volume capacity 50 mL, which was further heat treated at 180 °C for 24 h. Then the sediments were washed by centrifugation. The ferrite particles formed were, then, spread over silicon substrates by spin-coating procedure.

Bismuth oxide films were grown on ferrite particle layer in a low-pressure (200–260 Pa) flow type in-house built hot-wall atomic layer deposition (ALD) reactor in a two temperature ALD process. The process was started at 130 °C (10 cycles, only metal precursor pulse of 5 s and purge 5 s) and completed at 300 °C (250 cycles) using $BiCl_3$ (Aldrich, 99.99%) and O_3. Although the target stoichiometry of the films could be that of Bi_2O_3, considerable amounts of residual chlorine causing formation of solid bismuth oxychloride were measured. The thickness of bismuth oxide chloride films on nanoparticles as well as on the reference sample without nanoparticles was 5–10 nm.

Pieces of undoped Si(1 0 0) wafers as well as highly-doped Si covered by TiN layer were exploited as substrates. In the case of undoped Si (1 0 0), the native SiO_2 was removed using HF. The conducting substrates were based on (1 0 0)-oriented silicon with resistivity in the range of 0.014–0.020 Ω·cm, i.e., the Si substrates were boron-doped to concentrations up to 5×10^{18}..0.1×10^{19}/cm^3, and coated with 10 nm thick TiN layer pre-deposited using $TiCl_4/NH_3$ process in an ASM A412 Large Batch 300 mm reactor at Fraunhofer IPMS-CNT. The composite films for electrical measurements were also supplied with titanium-aluminum electrodes (area 0.204 mm^2) electron-beam evaporated on top of the films, with ca. 30 nm thick Ti layer in direct contact to the films.

Crystal structure was evaluated by grazing incidence X-ray diffractometry (GIXRD), using a X-ray diffractometer SmartLab Rigaku with CuK_α radiation and PDXL software for primary structural analysis. Surface morphology of particles and films was evaluated by scanning electron microscopy (SEM) using a Dual Beam equipment FEI Helios NanoLab 600. An X-ray fluorescence (XRF) spectrometer (Rigaku, ZSX 400) with the software program ZSX (version 5.55) was used to evaluate the elemental composition and thickness of the layers. Crystallite sizes were obtained using Williamson-Hall approximation integrated and after calculations provided by the same software. Electrical polarization measurements were performed by means of an Agilent DXO-X 3104 digital oscilloscope with a built-in wave generator. The standard Sawyer-Tower experiment was carried out by applying a periodic triangular-shaped stimulus and recording the voltage loops data from the oscilloscope. The values were obtained from the sensed voltage across a stated capacitance. Magnetic measurements were performed using Vibrating Sample Magnetometer (VSM) option of the Quantum Design 14 T Physical Property Measurement System by scanning the magnetic field from −50000 to +50000 Oe (from − 3979 to +3979 kA/m) parallel to the film surface at 5 K and at room temperature.

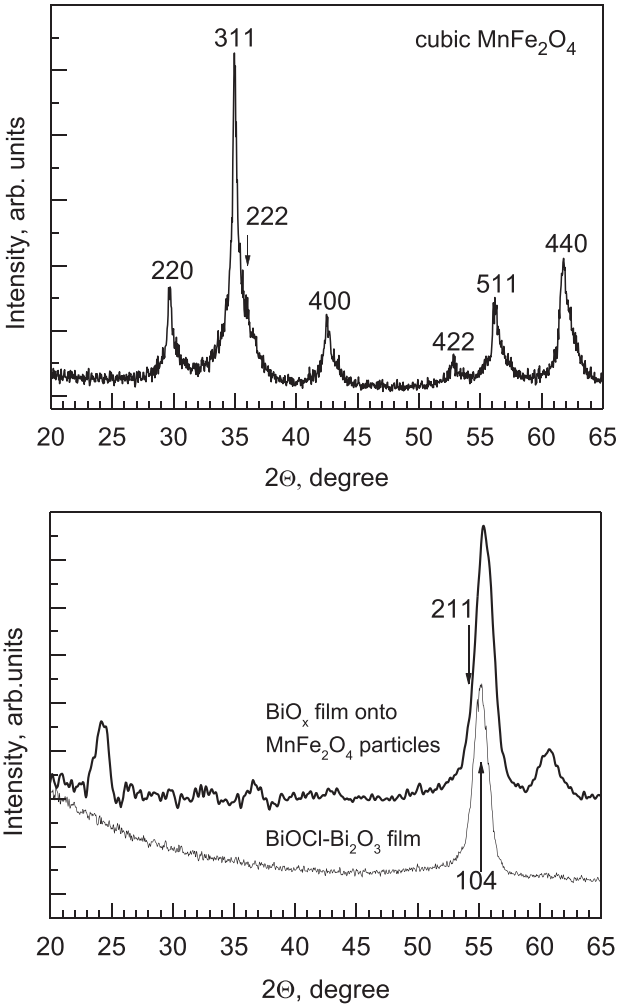

Fig. 1. Grazing incidence X-ray diffraction patterns of as-synthesized $MnFe_2O_4$ nanoparticles dip-coated over silicon substrate (upper panel), reference bismuth oxide chloride film (lower panel, lower curve), and bismuth oxide chloride deposited on ferrite nanoparticles (lower panel, upper curve) on titanium nitride covered silicon substrates. The reference 211 and 104 reflections from tetragonal BiOCl phase (Card 06-0249) are assigned.

3. Results and discussion

Fig. 1 depicts an X-ray diffractogram measured from the powder consisting of ferrite particles. The manganese ferrite particles were crystallized as synthesized. The reflections distinct in the pattern could, unambiguously, all be attributed to the cubic $MnFe_2O_4$ phase characteristic of the filed Jacobsite mineral (ICDD 01-073-3820, PDF 010-0319). The average size of the particles did not exceed 9–10 nm. Moreover, using an integrated Rigaku PDXL software with the Williamson-Hall method, the average $MnFe_2O_4$ crystallite size estimated was as small as 6–7 nm.

Rather similar structure has earlier been obtained in a study on the magnetic evolution of $Mn_xFe_{1-x}O$ nanoplates [11], where $Mn_xFe_{1-x}O$ nanoparticles required annealing in nitrogen atmosphere up to 380–450 °C, to transform ferrite with $Mn_{0.482}Fe_{0.508}O$ stoichiometry into spinel $MnFe_2O_4$. Furthermore, the 220, 311, 400, 422, 511, and 440 reflections of $MnFe_2O_4$, matching with those observed in the present study, were previously determined also in nanoparticles with sizes ranging from 4.6 to 8.2 nm, obtained by a solvothermal synthesis route from Mn and Fe acetylacetonate precursors [16].

In the diffractogram, measured from the reference 10 nm thick bismuth oxide chloride film as-deposited on planar silicon substrate,

only one intense, but broad reflection appeared at 55–51° (Fig. 1, lower panel). The intensity of the peak implies that the film was crystallized throughout its thickness, and the width of the peak indicates that the film is nanocrystalline, which is naturally expected at such low thicknesses. The phase crystallized could not be determined unambiguously on the basis of the pattern only. The exchange reaction between bismuth chloride and water could nominally result in the formation of bismuth oxide. Bismuth oxide, Bi_2O_3, has several equally strong reflections in its powder X-ray pattern (Card 029-0236), among which 223 and 621 at 54.3 and 55.5°, respectively, might overlap with the broad intense peak in the observed pattern (Fig. 1). However, in accord with the XRF analysis, the film deposited contained also considerable amounts of residual chlorine. It is known that, whenever chlorine or chloride is present in a system aiming at the production of bismuth oxides, rather stable bismuth oxide chloride, BiOCl, tends to form. BiOCl can often be formed purposefully, aiming at advanced catalysts [17–19]. In the reference film (Fig. 1), 211 and 104 reflections from tetragonal BiOCl (Card 06-0249) can be considered, ovelapping with the same broad peak extending over 54.1° and 55.1°. These reflections do not belong to the strongest ones in the powder diffraction pattern of BiOCl. Further, the film could be recrystallized into defined Bi_2O_3 structure upon agressive heating at 800 °C in air (pattern not shown). Nevertheless, the reference films in as-deposited state were most likely formed as nanocrystalline bismuth oxide chloride, BiOCl.

In general, XRD patterns measured from thin solid films can differ markedly from those considered as characteristic of polycrystalline bulk samples or powders of the same composition. All the reflections indexed in the filed powder diffraction cards may not appear in the patterns measured from thin films. In the case of thin film growth, texture together with preferred crystallographic orientations can develop during the deposition of the first few (tens of) nanometers in thickness. These phenomena may depend on the orientational effects of substrate, but also become affected by the precursor adsorption kinetics and nucleation densities. Thereby, the ordering in a nanomaterial can markedly depend on the synthesis routes to the material, and the structure of nanomaterials of the same composition but different morphology may not to be directly compared to each other. One can refer to the differences in the orientations of BiOCl based materials noticed earlier. For instance, in BiOCl nanosheets prepared by a wet chemical method as introduced by Guan et al. [20] and developed by Xu et al. [21], the 211 and 104 reflections in XRD patterns were clearly determined after a treatment procedure of the precursor oxychloride with polyetherimide [21], whereas in the untreated oxychloride sheets [20] these peaks were of insignificant intensity. Further, in $BiOCl/Bi_2O_3$ double-structured powders obtained after treatment of Bi_2O_3 particles in HCl [22] only the 104 reflection of BiOCl became visible nearby 50°in XRD patterns.

ALD of ca. 5 nm thick bismuth oxide chloride film on top of the layer of $MnFe_2O_4$ particles affected the crystalline structure of the ferrite particles remarkably (Fig. 1, lower panel). The main reflection from the bismuth oxide chloride phase at 55° was retained, however, implying that the oxides of metals constituting the film and the particles were not mixed in the form of ordered phases. At the same time, the reflections characteristic of spinel $MnFe_2O_4$ mostly disappeared. The resulting composite most likely consisted of a mixture of some disordered phases. Unambiguous phase determination became difficult, but a contribution from the cubic $Fe_{20.16}Mn_{11.84}O_{48.00}$ (card 900-7523) with 112 reflection at 23.1°, could not be neglected. Tetragonal $Mn_{10.81}Fe_{1.19}O_{16.00}$ (card 900-1966) with reflections 121 and 224 at 36.0° and 60.2°, respectively, might also add to the phase assemblage. Changes in the phase composition as well as in the stoichiometry of manganese ferrite based composites could be due to the effect of ALD of a film of foreign chemical composition at elevated temperature, i.e. at 300 °C. The surface of the nanoparticles is relatively large compared to their inner structure, which may make the particles somewhat fragile and less resistant to the influence of external thermal and mechanical influences able to deform the lattice.

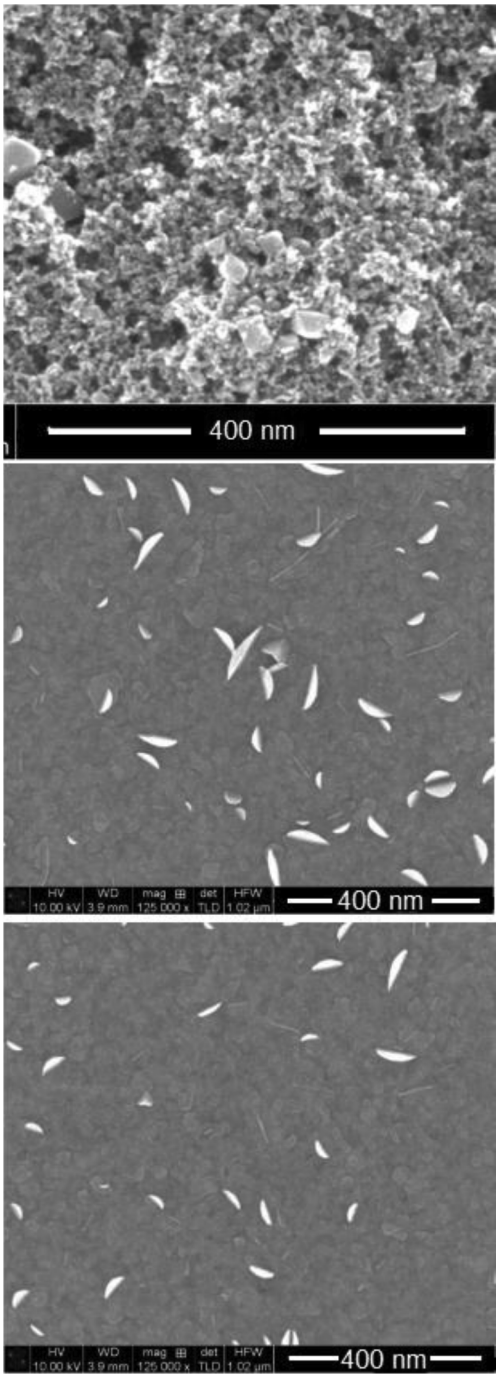

Fig. 2. Scanning electron microscope images from a spin-coated layer of $MnFe_2O_4$ nanoparticles (top panel), bismuth oxide layer deposited on nanoparticles (middle panel), and bismuth oxide film grown on silicon substrate without manganese ferrite particles (bottom panel).

SEM images of both non-coated and coated $MnFe_2O_4$ particles, as well as the bismuth oxide chloride based film, are presented in Fig. 2. One can see clearly, that the surface of layer consisting of $MnFe_2O_4$ particles only is covered by features characteristic of a rough, rather porous, layer, consisting of agglomerated grains. The average size of the single grains visible on the surface of the layer of nanoparticles could be estimated as small as 8–10 nm, on the basis of the SEM image.

The surface of the bismuth oxide chloride film is obviously much smoother. There appeared, however, certain needle-like features visible both on the bismuth oxide film and the nanocomposite surface covered

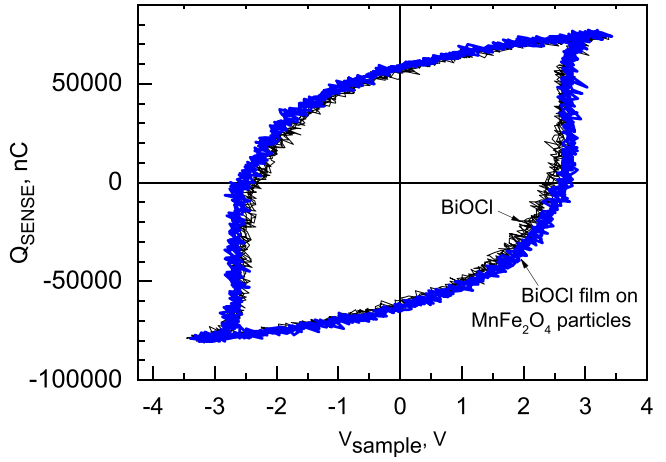

Fig. 3. Electrical charge versus applied voltage loops from a standalone ca. 10 nm thick bismuth oxide film and $MnFe_2O_4$ –BiOCl nanocomposite layer containing ca. 10 nm thick layer of manganese ferrite nanoparticles spin-coated on TiN/Si substrate.

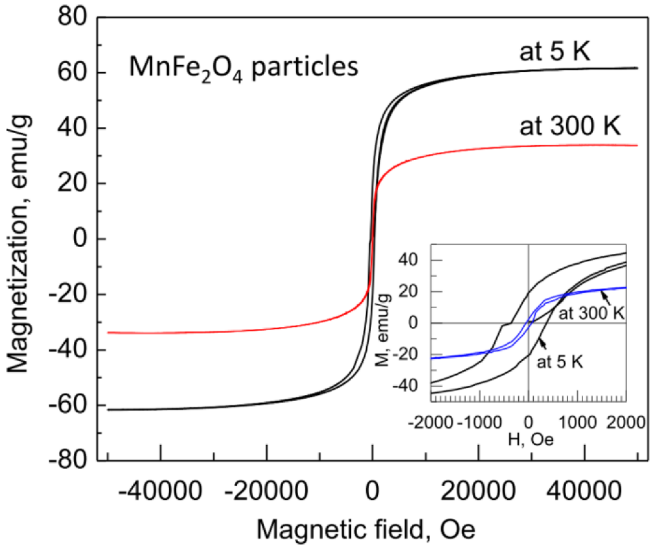

Fig. 4. Magnetization versus external magnetic field loops of layer of manganese ferrite particles measured at 3 K and at room temperature. The inset represents the loops around zero field in larger scale, in order to depict the differences in coercivity.

by the film. Such images probably reflect the structural ordering in the oxide chloride film, and analogous features have been observed on the surface of bismuth oxide chloride films previously [19].

In order to evaluate the nanocomposite as a continuous dielectric layer, electrical polarization (Fig. 3) in the films and nanocomposites was examined. Both the bismuth oxide chloride film and manganese ferrite particles covered by an oxide film demonstrated nonlinear polarization under alternating voltage polarity applied on the Al/Ti top and TiN/Si/Al bottom electrodes. The charge polarization – voltage loop remotely resembled that characteristic of ferroelectric material. One can notice rather weak tendency towards saturation of charge polarized at the extremal voltages. Rather significant role for the leakage currents through the nanomaterial is to be considered. There is an apparent remnant polarization measurable at zero voltage, up to 24.5–34.3 mC/cm^2, depending on the direction of the sample bias voltage sweep. The polarization is not yet to be approximated to that characteristic of ferroelectric material due to its high value compared to, e.g., 60 μC/cm^2 measured in 180 nm thick electron beam evaporated $BiFeO_3$ films [23], or to the value of about 10–30 μC/cm^2 estimated in metastable HfO_2-ZrO_2 based ferroelectric stacks [24,25]. A marked role for the charge likely trapped at electrode and/or internal interface defects is thus to be considered in the present case of BiOCl-$MnFe_2O_4$ composites. Earlier, the problem has been noticed and addressed, e.g., in the case of electrically leaky ferroelectric $Pb(Zr,Ti)O_3$ insulator layers by Meyer et al. [26]. Also in the present case, the charge trapped in the composite-film stack is gradually released during the oppositely polarized voltage pulses and, thus, interfacial polarization evidently dominates over the possible ferroelectric effect. The contribution of magnetic ferrite particles to the electrical polarization is evidently less important, because the characteristics of the polarization-voltage loops were similar in the case of both nanocomposites and the standalone BiOCl layer (Fig. 3). The strength of the electric field approximated to the coercive force, i.e., that required to decrease the polarization down to zero charge under opposite voltage, was similar in both cases, reaching 1.8 MV/cm. The hysteresis width is comparable to those obtained earlier in thin solid films grown to comparable thicknesses [23–26].

Fig. 4 depicts magnetic behavior of $MnFe_2O_4$ powder expressed by magnetization-field loops measured from the nanoparticles in powder without bismuth oxide chloride film. The magnetization curves resemble those otherwise characteristic of soft ferromagnetic materials. Both saturation magnetization and coercive force increased markedly with the decrease in the measurement temperature. The saturation magnetization, M_S, was 33.8 emu/g at room temperature, and increased to 61.7 emu/g at 5 K. The coercivity, H_C, was lower than 50 Oe at the room temperature, increasing to 370 Oe at 5 K (Fig. 4). $MnFe_2O_4$ nanoparticles have earlier been described as materials with small magnetocrystalline anisotropy and easy magnetization reversal [5] which is the likely reason for the narrow hysteresis and weak coercivity of this compound in its nanocrystalline form.

According to the literature data, $MnFe_2O_4$ nanocrystals have earlier shown small but finite magnetic hysteresis behavior with coercivity being a function of their size [10]. Field-dependent magnetization of $MnFe_2O_4$ nanocrystals has been measured earlier at 5 K [10]. As the size of $MnFe_2O_4$ nanocrystals increased, the coercivity of the $MnFe_2O_4$ nanocrystals increased almost linearly [10]. For further comparison, Liu et al. [7] observed definitively superparamagnetic behavior in $MnFe_2O_4$ spinel ferrite nanocrystallites measurable with ca. 8 nm in diameter, produced by a reverse micelle synthesis route. In the latter case, the remnant magnetization ceased already at temperatures significantly lower than room temperature. Also in another study on $MnFe_2O_4$ superparamagnetic nanocrystallites measurable to ca. 10 nm in diameter, obtained also through reverse micelle synthesis [8], certain hysteresis in M − H curves was followed when measured at 2 K, whereas at 300 K the hysteresis and coercivity ceased and the material started to behave as a (super)paramagnetic material.

Superparamagnetic behavior is often expected in the case of small particles of magnetic materials. Saturative magnetization in the present study was, however, observed at room temperature. The mass susceptibility was measured in non-covered nanoparticles against the measurement temperature in a small applied field (Fig. 5). The maximum value of the susceptibility, χ_{max}, of 0.055 emu(g^{-1} Oe^{-1}) was recorded at 126.7 K in the zero field cooled regime (Fig. 5). At room temperature, the value of χ was still as high as 0.048 emu(g^{-1} Oe^{-1}). The maximum could be approximated to the blocking temperature commonly characteristic of superparamagnetic nanoparticles with size measured in few nanometers [27]. For the comparison to literature data, the blocking temperatures of various $MnFe_2O_4$ nanocrystals [10] have increased with the size of the nanocrystals. As the diameter of the nanocrystals changed from 4.5 to 12 nm, their corresponding blocking temperatures rose from 32 to 123 K [10]. In the present study, the blocking temperature value of 126 K characteristic of crystallites with sizes at approximately 10 nm is, thus, roughly in agreement with the results obtained previously.

The layer of manganese ferrite particles covered by the bismuth

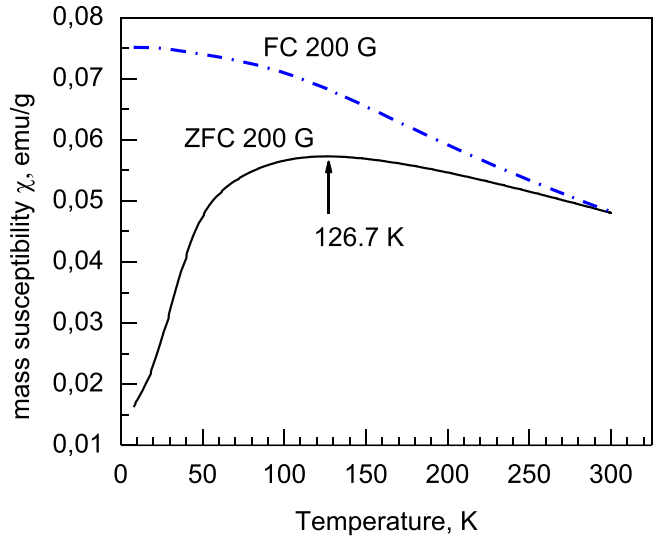

Fig. 5. Field cooled (FC) and zero-field cooled (ZFC) susceptibility curves measured from $MnFe_2O_4$ nanoparticles.

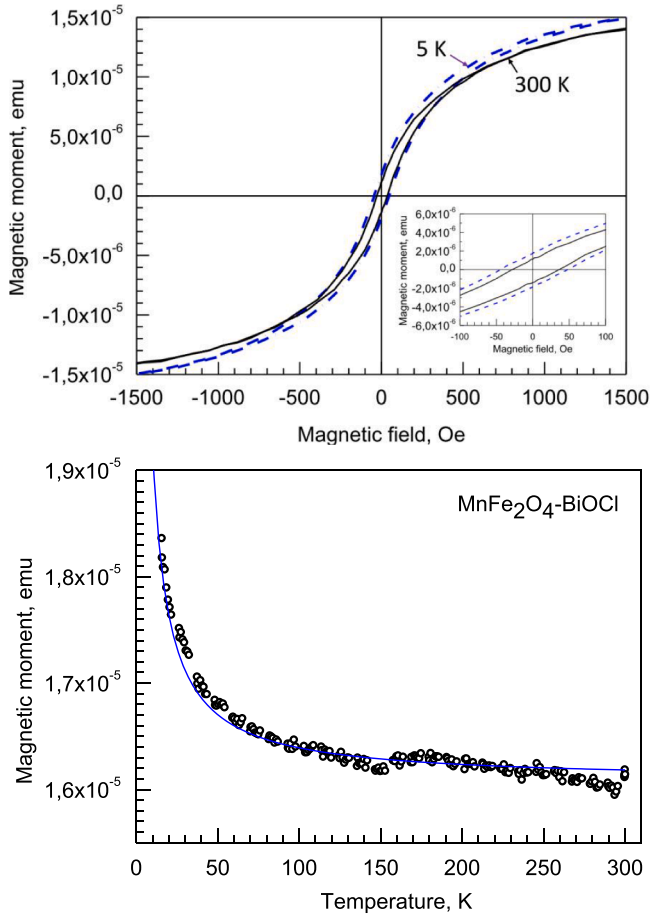

Fig. 6. Magnetic moment versus magnetic field loop measured at room temperature and at 5 K (upper panel), and temperature dependent susceptibility curve (lower panel) in $MnFe_2O_4$-BiOCl nanocomposite layer formed on TiN/Si substrate. Solid line in the lower panel reflects the result of fitting in accord with Curie plot.

oxide chloride film also exhibited nonlinear magnetization in external magnetic field at room temperature and tendency to saturate at higher fields (Fig. 6), although the structure of the crystallites was markedly affected by the deposition of bismuth oxide chloride, as described above. One could see, that the polarization saturated at sufficiently high fields in both opposite magnetic field directions (high fields are not shown), accompanied with measurable hysteresis in the magnetization-field curves. The hysteresis width allowed one to estimate coercivity around 30 Oe, i.e., which is still close to the values characteristic of soft ferromagnetic materials. The values of both coercivity and saturation magnetization increased only slightly at low temperatures, as measured at 5 K (Fig. 6).

Temperature-dependent susceptibility curve of the nanocomposite (Fig. 6) did not indicate superparamagnetic behavior as was in the case $MnFe_2O_4$ nanopartcles (Fig. 5) and thus a blocking temperature [27] could not be assigned. Instead, a paramagnetic Curie contribution dominated in the low temperature range.

It was shown by the XRD that the crystalline structure of the ferrite particles changed noticeably after the deposition of the bismuth oxide chloride film, and the resulting nanocomposite consisted of a mixture containing disordered phases. Magnetometry data could not identify the ambiguous phases but demonstrated that at least some of them have paramagnetic nature while others demonstrate ferro- or ferrimagnetic behavior.

In our present study, the bismuth oxide chloride film alone did not exhibit saturation and hysteresis in the magnetization behavior. One can note, that even nearly stoichiometric (in terms of the bismuth to iron atomic ratio) $BiFeO_3$ alone grown by ALD earlier could not possess significant hysteresis in M−H curves [28]. In order to induce and observe coercivity in magnetization-field loops at room temperature, iron-rich bismuth iron oxide layers had to be grown by ALD [29].

In the present work, no traces of bismuth ferrites were recognized in the structure of nanocomposites. It is thus unlikely that the ALD process involving surface reactions with bismuth chloride have affected the elemental composition of underlying ferrite particles at the reactor temperature of 300 °C. Instead, as supposed above, nucleation and formation of manganese-rich ferrite phases with stoichiometry markedly different from that of $MnFe_2O_4$, can not be excluded. The exact determination of the phase composition after the film deposition process turned out to be still impossible, due to the absence of distinctive characteristic peaks in the diffraction patterns. However, possible destruction of the main spinel structure must noticeably influence the magnetic response of the material. Decrease in the magnetization and coercivity should, in the present case, be caused by disordering of the lattice of the solid ferrite material. Structural changes would thus affect the magnetocrystalline anisotropy and, concurrently, the coercive field as described above.

A previous study on solvothermally from metal acetylacetonates synthesized manganese ferrites [16] has described of manganese ferrite particles based materials exhibiting magnetic performance similar to that observable in the present study. Besides $MnFe_2O_4$, also $Mn_{0.77}Fe_{2.23}O_4$ and α-Fe_2O_3 phases could coexist in the particles [16]. In the latter case the magnetization, as measured, was weaker compared to that characteristic of pure spinel particles. The coercive forces in two-phase materials did not differ significantly from those measured in $MnFe_2O_4$ nanoparticles. It is still possible that polarization reversal in nanocrystalline grains with multiphase structure and, concurrently, disordered lattice is easier and therefore the coercive force slightly weaker. This would, plausibly, explain the moderate decrease in the coercivity in the BiOCl-$MnFe_2O_4$ composites, compared to $MnFe_2O_4$ particles, as described above.

4. Summary

$MnFe_2O_4$ nanoparticles with spinel structure and with diameter about 10 nm were successfully synthesized via wet chemical route and transferred to the planar silicon substrates using spin coating technique. The particles exhibited magnetization characteristic of ferromagnetic materials with coercivity up to 70 Oe at room temperature. Although the particles also demonstrated behavior characteristic of

superparamagnetic material, finite hysteresis width and marked saturation in magnetic polarization curves were retained at room temperature and below that.

The bismuth oxide (chloride) film was deposited in order to provide continuity of the layers and avoid short circuits between electrical contacts provided by substrate and evaporated gate electrodes. In addition, the bismuth oxide based layer could contribute to the electrical polarization without its possible deterioration after interfacial reactions between oxides constituting the nanocomposite. As a result, polarization charge versus electric field loops could be measured. The polarization was, likely, overwhelmed by the leakage and interfacial effects. Nonetheless, weak implications of ferroelectric component were nevertheless observed in the electrical behavior of the nanocomposite. The half-width of the hysteresis in the charge-voltage loops, approximated to the coercivity, extended to 1.8 MV/cm. The manganese ferrite – bismuth oxide (chloride) based nanocomposites appeared to be measurable in magnetic and electric fields and exhibited polarization in both cases.

Declaration of Competing Interest

The authors declare that they have no known competing financial interests or personal relationships that could have appeared to influence the work reported in this paper.

Acknowledgements

The authors are thankful to Profs. Helena Castán and Salvador Dueñas, University of Valladolid, for providing the electrical evaluation of the continuous film and nanocomposite and to mr. Aivar Tarre, University of Tartu for consultations on X-ray analysis. The study has partially been supported by the European Regional Development Fund project “Emerging orders in quantum and nanomaterials” (TK134), and Estonian Research Agency (PRG4).

References

[1] J.S. Andrew, J.D. Starr, M.A.K. Budi, Prospects for nanostructured multiferroic composite materials, Scripta Mater. 74 (2014) 38–43, https://doi.org/10.1016/j.scriptamat.2013.09.023.

[2] J.-R. Huang, C. Cheng, Cation and magnetic orders in $MnFe_2O_4$ from density functional calculations, J. Appl. Phys. 113 (2013) 033912, , https://doi.org/10.1063/1.4776771.

[3] N.A. Spaldin, Magnetic Materials. Fundamentals and Applications, Second ed., Cambridge University Press, 2011 ISBN 9780511900716.

[4] H. Yang, C. Zhang, X. Shi, H. Hu, X. Du, Y. Fang, Y. Ma, H. Wu, S. Yang, Water-soluble superparamagnetic manganese ferrite nanoparticles for magnetic resonance imaging, Biomaterials 31 (2010) 3667–3673, https://doi.org/10.1016/j.biomaterials.2010.01.055.

[5] N.A. Frey, S. Peng, K. Cheng, S. Sun, Magnetic nanoparticles: synthesis, functionalization, and applications in bioimaging and magnetic energy storage, Chem. Soc. Rev. 38 (2009) 2532–2542, https://doi.org/10.1039/b815548h.

[6] C.R. Vestal, Z.J. Zhang, Effects of surface coordination chemistry on the magnetic properties of $MnFe_2O_4$ spinel ferrite nanoparticles, J. Am. Chem. Soc. 125 (2003) 9828–9833, https://doi.org/10.1021/ja035474n.

[7] C. Liu, B. Zou, A.J. Rondinone, Z.J. Zhang, Reverse micelle synthesis and characterization of superparamagnetic $MnFe_2O_4$ spinel ferrite nanocrystallites, J. Phys. Chem. B 104 (2000) 1141–1145, https://doi.org/10.1021/jp993552.

[8] E.E. Carpenter, C.J. O'Connor, V.G. Harris, Atomic structure and magnetic properties of MnFe2O4 nanoparticles produced by reverse micelle synthesis, J. Appl. Phys. 85 (1999) 5175–5177, https://doi.org/10.1063/1.369115.

[9] M. Bellusci, S. Canepari, G. Ennas, A.L. Barbera, F. Padella, A. Santini, A. Scano, L. Seralessandri, F. Varsano, Phase evolution in synthesis of manganese ferrite nanoparticles, J. Am. Ceram. Soc. 90 (2007) 3977–3983, https://doi.org/10.1111/j.1551-2916.2007.02061.x.

[10] Q. Song, Y. Ding, Z.L. Wang, Z.J. Zhang, Tuning the thermal stability of molecular precursors for the nonhydrolytic synthesis of magnetic $MnFe_2O_4$ spinel nanocrystals, Chem. Mater. 19 (2007) 4633–4638, https://doi.org/10.1021/cm070990o.

[11] H.-M. Song, J.I. Zink, N.M. Khashab, Selective magnetic evolution of $Mn_xFe_{1-x}O$ nanoplates, J. Phys. Chem. C 119 (2015) 10740–10748, https://doi.org/10.1021/acs.jpcc.5b01938.

[12] C.N. Chinnasamy, Aria Yang, S.D. Yoon, Kailin Hsu, M.D. Shultz, E.E. Carpenter, S. Mukerjee, C. Vittoria, V.G. Harris, Size dependent magnetic properties and cation inversion in chemically synthesized $MnFe_2O_4$ nanoparticles, J. Appl. Phys. 101 (9) (2007) 09M509 http://aip.scitation.org/doi/10.1063/1.2710218https://doi.org/10.1063/1.2710218.

[13] A. Kumar, K.L. Yadav, Synthesis and characterization of $MnFe_2O_4$–$BiFeO_3$ multiferroic composites, Phys. B 406 (2011) 1763–1766, https://doi.org/10.1016/j.physb.2011.02.023.

[14] N.M. Aimon, D.H. Kim, X.Y. Sun, C.A. Ross, Multiferroic behavior of templated $BiFeO_3$ − $CoFe_2O_4$ self-assembled nanocomposites, ACS Appl. Mater. Interfaces 7 (2015) 2263–2268, https://doi.org/10.1021/am506089c.

[15] A.A. Dakhel, Hydrogen influenced the structural and optical properties of Ni-doped BiOCl nanocomposite: creation of FM properties, Appl. Phys. A 125 (2019) 89, https://doi.org/10.1007/s00339-019-2393-3.

[16] K. Vamvakidis, D. Sakellari, M. Angelakeris, C. Dendrinou-Samara, Size and compositionally controlled manganese ferrite nanoparticles with enhanced magnetization, J. Nanopart. Res. 15 (2013) 1743, https://doi.org/10.1007/s11051-013-1743-x.

[17] E.L. Cuellar, J.O. Cortéz, A.M. de la Cruz, A.G. Loera, U.O. Méndez, Photocatalytic activity of BiOCl thin films deposited by thermal evaporation, Thin Solid Films 659 (2018) 57–63, https://doi.org/10.1016/j.tsf.2018.04.044.

[18] X. Zhang, R. Li, Y. Wang, X. Zhang, Y. Wang, C. Fan, Slow-releasing Cl^- to prepare BiOCl thin film on Bi plate and its photocatalytic properties, Mater. Lett. 174 (2016) 126–128, https://doi.org/10.1016/j.matlet.2016.03.109.

[19] H. Peng, C.K. Chan, S. Meister, X.F. Zhang, Y. Cui, Shape evolution of layer-structured bismuth oxychloride nanostructures via low-temperature chemical vapor transport, Chem. Mater. 21 (2009) 247–252, https://doi.org/10.1021/cm802041g.

[20] M.L. Guan, C. Xiao, J. Zhang, S.J. Fan, R. An, Q.M. Cheng, J.F. Xie, M. Zhou, B.J. Ye, Y. Xie, Vacancy associates promoting solar-driven photocatalytic activity of ultrathin bismuth oxychloride nanosheets, J. Am. Chem. Soc. 135 (2013) 10411–10417, https://doi.org/10.1021/ja402956f.

[21] Y. Xu, Z. Shi, L. Zhang, E.M.B. Brown, A. Wu, Layered bismuth oxyhalide nanomaterials for highly efficient tumor photodynamic therapy, Nanoscale 8 (2016) 12715–12722, https://doi.org/10.1039/c5nr04540a.

[22] S.Y. Chai, Y.J. Kim, M.H. Jung, A.K. Chakraborty, D. Jung, W.I. Lee, Heterojunctioned $BiOCl/Bi_2O_3$, a new visible light photocatalyst, J. Catal. 262 (2009) 144–149, https://doi.org/10.1016/j.jcat.2008.12.020.

[23] H. Naganuma, Y. Inoue, S. Okamura, Evaluation of ferroelectric hysteresis loops of leaky multiferroic $BiFeO_3$ films using a system with a high driving frequency of 100 kHz system, J. Ceram. Soc. Jpn. 118 (2010) 656–658, https://doi.org/10.2109/jcersj2.118.656.

[24] A. Onodera, M. Takesada, Ferroelectricity in simple binary crystals, Crystals 7 (2017) 232, https://doi.org/10.3390/cryst7080232.

[25] J. Müller, T.S. Böscke, U. Schröder, S. Mueller, D. Bräuhaus, U. Böttger, L. Frey, T. Mikolajick, Ferroelectricity in simple binary ZrO_2 and HfO_2, Nano Lett. 12 (2012) 4318–4323, https://doi.org/10.1021/nl302049k.

[26] R. Meyer, R. Waser, K. Prume, T. Schmitz, S. Tiedke, Dynamic leakage current compensation in ferroelectric thin-film capacitor structures, Appl. Phys. Lett. 86 (2005) 142907, , https://doi.org/10.1063/1.1897425g.

[27] I.J. Bruvera, P.M. Zélis, M.P. Calatayud, G.F. Goya, F.H. Sánchez, Determination of the blocking temperature of magnetic nanoparticles: the good, the bad, and the ugly, J. Appl. Phys. 118 (2015) 184304, , https://doi.org/10.1063/1.4935484.

[28] C.D. Pham, J. Chang, M.A. Zurbuchen, J.P. Chang, Synthesis and characterization of $BiFeO_3$ thin films for multiferroic applications by radical enhanced atomic layer deposition, Chem. Mater. 27 (2015) 7282–7288, https://doi.org/10.1021/acs.chemmater.5b02162.

[29] M. Puttaswamy, M. Vehkamäki, K. Kukli, M.C. Dimri, M. Kemell, T. Hatanpää, M.J. Heikkilä, K. Mizohata, R. Stern, M. Ritala, M. Leskelä, Bismuth iron oxide thin films using atomic layer deposition of alternating bismuth oxide and iron oxide layers, Thin Solid Films 611 (2016) 78–87, https://doi.org/10.1016/j.tsf.2016.05.006.